Microdisk resonator filters made of dielectric-loaded plasmonic waveguides

Odysseas Tsilipakos, Emmanouil E. Kriezis

Department of Electrical and Computer Engineering, Aristotle University of Thessaloniki, Thessaloniki GR-54124, Greece

Abstract

Microdisk resonator filters, an alternative to microring resonator filters, are studied by means of vectorial three dimensional finite element method simulations. Their performance characteristics are highlighted for different microdisk radii, and compared with those of the respective, footprint-wise, microring filters. We show that microdisk filters are advantageous, as the resonator involved exhibits smaller radiation losses. Extinction ratios as high as 30 dB are possible by properly tuning the gap separating the waveguide from the microdisk in each case. Transmission dips due to higher-radial-order modes that drastically change the transmission picture appear only for very large microdisk radii.

Keywords: surface plasmon polaritons, dielectric-loaded plasmonic waveguide, optical resonators, optical filters, integrated optics

Email addresses: otsilipa@auth.gr (Odysseas Tsilipakos), mkriezis@auth.gr (Emmanouil E. Kriezis)

1. Introduction

Surface plasmon polaritons (SPPs) are electromagnetic surface waves coherently coupled to collective oscillations of a metal's free electron density [1]. SPPs are supported by suitable plasmonic waveguides comprising at least one metal-dielectric interface and can have a lateral spatial extent of sub-wavelength dimensions. As a result, plasmonic components are a prime candidate for nanophotonic integrated circuits, combining the bandwidth of photonics along with nanoscale dimensions [2–6].

The stripe waveguide was the first 2D plasmonic waveguide, i.e., able to confine light in both transverse directions, to be extensively investigated. It has been employed in the implementation of various plasmonic components [7, 8]. However, the long-range mode supported by the stripe waveguide lacks strong lateral confinement and new 2D plasmonic waveguides were sought for in the following years featuring subwavelength confinement and therefore being suitable for densely integrated plasmonic circuits.

The recently proposed dielectric-loaded plasmonic (DLSPP) waveguide [9] offers some distinct advantages compared to other alternatives. It is technologically simple, it exhibits strong guiding properties while featuring tolerable propagation losses, and it can readily accommodate different loading materials therefore presenting a means of providing DLSPP-based components with tuning capabilities. Among the DLSPP-based plasmonic components that have been demonstrated [10–15], wavelength-selective components are of substantial interest, since they can provide the necessary functionalities needed to assemble fully operational plasmonic circuits.

2. Microdisk resonator filters

In this work, we focus on DLSPP-based microdisk resonator filters, an alternative to microring resonator filters which have been studied elsewhere [13–15]. Microdisk resonator filters are wavelength-selective components composed of a bus waveguide coupled to a microdisk resonator. The microdisk resonator is a traveling wave resonator just like the microring, with the difference that it supports whispering gallery modes, instead of circulating modes of the underlying bent waveguide. Microdisk and microring resonators are widely used in other photonics technologies [16–19] for filtering, multiplexing and switching purposes .

Microdisk filters are worth investigating because of mainly three reasons. Firstly, microdisk resonators feature smaller radiation losses (termed bend losses in microring context), and therefore higher quality factors, compared to microring resonators of the same outer radius. This is because in microdisk resonators the absence of an inner cylindrical boundary permits the supported mode to reside closer to the resonator center. In other words, the field components feature weaker penetration in the surrounding air and the supported mode exhibits stronger confinement. As a result, narrower minima linewidths and higher transmission maxima are anticipated, when ring and disk filters of the same footprint are compared. This should be pronounced in the cases where the radiation losses are significant, i.e., for small radii. On a fabrication level reduced scattering losses due to surface roughness are expected as well, since there is only one boundary cylindrical surface. Secondly, the inherent ability of disks to support higher-radial-order modes can drastically alter the transmission picture, provided, of course, that these are

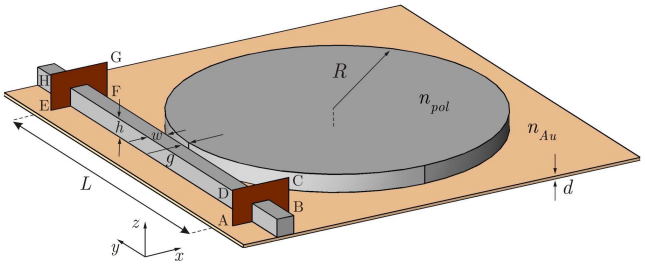

Figure 1: (Color on web only) Schematic of a DLSPP-based microdisk resonator filter. The cross-section at which the output power is calculated is marked as EFGH and is separated by a distance $L = 2R$ from plane ABCD at which the reference power is calculated.

effectively excited. Finally, microdisk filters seem to be more amenable to optical addressing. Then, by focusing a control light beam on the disk surface, dynamically controlled microdisk resonator filters can be realized.

2.1. Structural layout

The performance of DLSPP-based microdisk resonator filters is investigated by means of vectorial three-dimensional finite element method (3D-FEM) simulations. All simulations were conducted by using in-house code. The details of the finite element method implementation are described in Ref. [15]. A schematic of the simulated structure is depicted in Fig. 1. Once the electric field in the entire structure is obtained, the filter transmission can be calculated by collecting the guided power propagating past the microdisk (plane EFGH) and normalizing with respect to a reference power level computed in the absence of the disk at plane ABCD. The two planes are separated by a distance $L = 2R$. Clearly, this length L imposes an upper bound on the filter transmission. Concerning the material properties, the polymer has a typical refractive index of 1.5362, and the dielectric permit-

tivity of gold is obtained by linear interpolation between the measured values reported in Ref. [20]. As for the geometrical parameters, the bus waveguide is made of a $w \times h = 600 \times 600$ nm^2 polymer ridge, ensuring the single-mode operation of the DLSPP waveguide in the wavelength range of interest [9]. We adopt the same height (600 nm) for the microdisk as well. The gold film is $d = 100$ nm thick. The remaining geometrical parameters are the gap separating the waveguide from the disk (measured between the edges of the two), g, and the disk radius R. They are the ones that mainly affect the filter response, and will be regarded as design parameters.

2.2. Study of filter response

Obviously, there are two distinct loss mechanisms present in DLSPP-based microdisk resonator filters: radiation losses, i.e., power leaving the resonator by coupling to outward-propagating radial radiation modes and resistive losses in the metallic film. Depending on the disk radius these loss mechanisms contribute differently to the overall resonator losses. We identify two operating regimes for the resonator. Specifically, in the small-radius regime the radiation losses are significant and play a prominent role in shaping the filter response. On the other hand, for large radii the radiation losses are negligible and it is the resistive losses alone that determine the filter performance. In what follows, typical examples highlighting the performance characteristics of filters belonging in the aforementioned regimes will be presented.

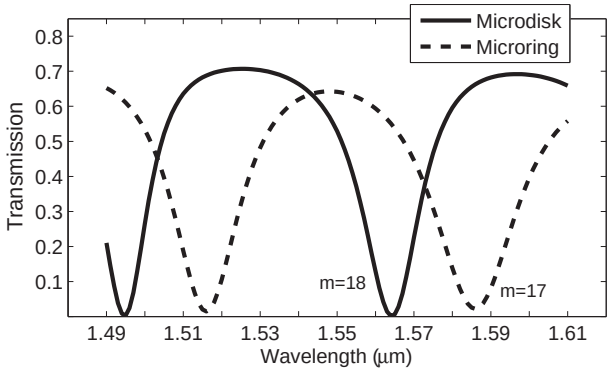

Figure 2: Transmission vs wavelength for a critically coupled microdisk resonator filter with a disk radius of 3.8 μm and a gap of 0.1 μm. The transmission of the respective, footprint-wise, critically coupled microring resonator filter ($R = 3.5$ μm, $g = 0.1$ μm) is also included for comparison purposes.

2.2.1. Small radii: Microdisk superiority

Let us first consider a microdisk filter belonging in the small-radius regime. A disk radius of 3.8 μm is chosen, for a direct comparison with the 3.5 μm-microring case studied in Ref. [15] to be possible. We found that the gap should be set to 0.1 μm for the disk to be critically coupled to the bus waveguide. At critical coupling the transmission minima approach zero and the extinction ratio is greatly improved. The filter transmission is depicted in Fig. 2 along with the transmission of the respective, footprint-wise, microring filter (In the microring case the radius R refers to the fictitious circumference located midway between the inner and outer ring boundaries). We note that the neighboring minima of the two transmission curves are induced by modes of different azimuthal order m, due to the different effective circumference that the modes of the microdisk and the microring experience. Clearly, the quality factors of the resonances in the microdisk case are higher, since

the linewidths of the respective transmission minima are narrower. To back this up we performed eigenvalue simulations for the uncoupled resonators. Indeed, the quality factor of a microdisk resonance is approximately 182, almost double the one of a microring resonance which is approximately 96. Alternatively, this implies that if a certain quality factor is sought for, it can be provided by a microdisk that is more compact than the same-Q microring. The higher quality factors can be attributed to the reduced radiation losses, since the resistive losses are roughly the same in both cases.

In order to provide physical insight into the reduced radiation losses of microdisk resonators revealed by the rigorous 3D-FEM simulations, we decided on performing some additional calculations. Specifically, we start by calculating the effective radius R_{eff} that the supported modes experience. R_{eff} is the radial distance between the supported mode's peak (E_z component) and the center of the resonator. Alternatively, $2\pi R_{eff}$ is the circumferential path traveled by the peak of the mode. For the $m = 17$ microring minimum at $\lambda = 1.586$ μm we find $R^R_{eff} = 3.575$ μm. The effective radius is larger than 3.5 μm, i.e., the center of the bent waveguide, indicating that the peak of the circulating mode is shifted toward the outside of the resonator, as one would expect. For the $m = 18$ microdisk resonance at $\lambda = 1.564$ μm we find $R^D_{eff} = 3.506$ μm. As stated in the introductory section, the absence of the inner cylindrical boundary allows the supported mode to reside closer to the resonator center ($R^D_{eff} < R^R_{eff}$). Subsequently, we calculate the corresponding effective indexes (real parts), by making use of the resonance condition, through:

$$n^{R/D}_{eff}(\lambda_m) = \frac{m\lambda_m}{2\pi R^{R/D}_{eff}(\lambda_m)}. \quad (1)$$

For the microring case we find $n_{eff}^{R} = 1.2$. As the corresponding value for the straight waveguide is 1.287 we again infer that the mode of the bent waveguide is shifted and less confined, as one would expect. For the microdisk case we calculate $n_{eff}^{D} = 1.278$. Strictly speaking, an effective index can not be appointed to the microdisk resonance since there is no underlying waveguide. It is exercised only for comparison purposes. We observe that $n_{eff}^{D} > n_{eff}^{R}$ indicating that the field components of the microdisk mode do not penetrate as much in the surrounding air. The comparisons made between microdisk/ring resonators for both quantities (R_{eff} & n_{eff}) provide a physical interpretation of the reduced radiation losses featured by microdisk resonators. Finally, we should note that we decided on comparing the neighboring instead of the same-azimuthal-order resonances because R_{eff} and n_{eff} exhibit dispersion, i.e., they are functions of frequency.

Returning to Fig. 2, we observe that the maximum transmission value is higher in the microdisk case; another consequence of the reduced losses. The extinction ratio is $\sim$ 30 dB and the free spectral range (FSR) is $\sim$ 70 nm. As can be seen, no transmission dips due to higher-radial-order modes are present. Since eigenvalue simulations reveal that higher-radial-order modes do exist, we attribute this fact to the poor excitation of these modes.

2.2.2. Large radii: Disk and ring equivalence

Subsequently, a microdisk filter with a disk radius of 5.3 μm is considered. For such a large radius the resistive losses have fully dominated and solely determine the overall losses. This time a gap of 0.15 μm is needed for critical coupling to hold. The transmission for this case is depicted in Fig. 3, along with the transmission of the respective, footprint-wise, critically cou-

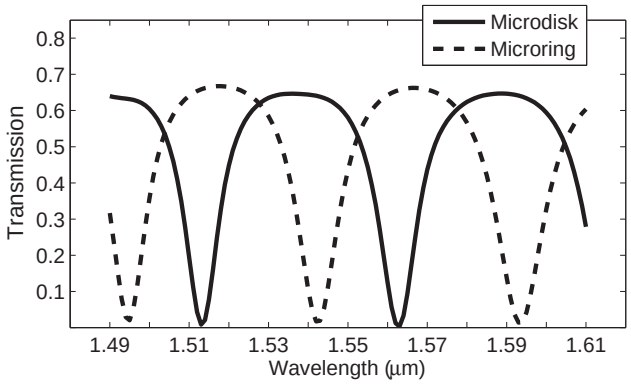

Figure 3: Transmission vs wavelength for a critically coupled microdisk resonator filter with a disk radius of 5.3 μm and a gap of 0.15 μm. The transmission of the respective, footprint-wise, critically coupled microring resonator filter ($R = 5.3$ μm, $g = 0.2$ μm) is also included for comparison purposes.

pled microring resonator filter ($R = 5.0$ μm, $g = 0.2$ μm). The FSR is ~ 50 nm, and the extinction ratio ~ 25 dB. We note that now the advantage of the microdisk compared to the microring filter is not as pronounced, since the resistive losses fully dominate in this large-radius case. Specifically, a typical quality factor for a microdisk resonance is ~ 258 compared to ~ 220 for a resonance of the corresponding microring. Again, no transmission dips due to higher-radial-order modes are present, although such modes do exist as eigenvalue simulations reveal. However, they do become visible if we repeat the simulation adopting a purely real dielectric permittivity for gold, as the transmission dips induced by the first-radial-order modes become narrower and the maximum transmission higher. Therefore, one can infer that higher-radial-order modes are on the verge of starting to become excited.

2.2.3. Very large radii: Second radial order modes

In an attempt to demonstrate microdisk resonator filters featuring transmission dips induced by higher-radial-order modes, we decided on examining filters with disks of even larger radii. We found that it is for disk radii larger than 6.3 μm that transmission dips induced by second-radial-order modes clearly make their appearance. Thus, the radius value of 6.3 μm can be considered as a second-radial-order-dip threshold, past which second-radial-order modes are efficiently excited. However, we should note that this threshold depends not only on the disk radius, but on the mode width of the bus waveguide (and therefore its geometrical width) as well. If a different waveguide width is adopted, the mode matching condition between the straight waveguide mode and the second-radial-order mode of the microdisk will begin to hold for a somewhat different radius. Although this limits the significance of the threshold just specified, it also, and more importantly, means that the waveguide width is a valuable degree of freedom in tailoring the excitation efficiency of second-radial-order modes and therefore the transmission curve (Fig. 4).

In Fig. 4 the transmission of a 6.8 μm-radius microdisk resonator filter is depicted. The case of a filter with a 0.5 μm-wide straight waveguide is also included in order to demonstrate the effect of the waveguide width on the excitation efficiency of the second-radial order modes. We found that the gap should be set to 0.1 μm, for critical coupling of the first-radial-order modes to hold. This time, transmission dips due to second-radial-order modes are clearly visible, substantially modifying the FSR and drastically changing the transmission picture. This unique feature of microdisk filters is of extra

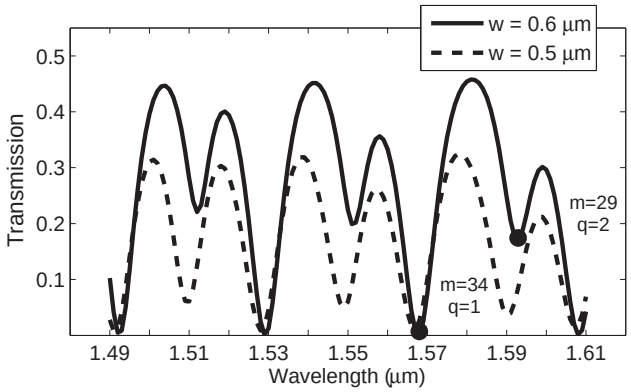

Figure 4: Transmission vs wavelength for a microdisk resonator filter with a disk radius of 6.8 μm and a gap of 0.1 μm. Two values for the straight waveguide width, namely 0.6 and 0.5 μm, are considered. Transmission dips due to second-radial-order modes ($q = 2$) are clearly visible.

importance in plasmonics context considering that one can not obtain small FSRs (< 30 nm) with microring filters by simply using larger-radius rings, something easily done in semiconductor photonics technologies for example [17], due to the high resistive losses that accompany them. We also note that the maximum transmission is lower than in the previous cases; a consequence of the high resistive losses associated with the large circumference of the disk and the length separating the input and output ports as well as the position of the second-radial-order mode transmission dips. Specifically, the maximum transmission is roughly 0.46, as opposed to ~ 0.71 and ~ 0.65 of the previous cases. One can consider the 6.8 μm-case as a limiting one. For radii above 6.8 μm the resistive losses become quite large, degrading the filter performance. On the other hand, for small radii, below 3 μm, it is the radiation losses that become prohibitive. Even if one could tolerate the wider minima linewidths and the higher insertion losses associated with resonators of high overall

losses, technological challenges would have to be overcome as well, since very small gaps, in the order of tens of nanometers, would be required for critical coupling to hold.

In Fig. 5 the real part of E_z is depicted at transmission minima induced by a first ($q = 1$) and a second-radial-order ($q = 2$) mode. The corresponding modes of the uncoupled resonator are also included. Obviously, the azimuthal order m of the two modes is different, since the second-radial-order mode must fit on a circumference that is closer to the center of the disk and therefore smaller. We note that at the $\lambda = 1.593$ μm transmission minimum, which is induced by a second-radial-order mode, a first-radial-order mode ($m = 33$) is also excited, albeit not as efficiently, and the net result [Fig. 5(b)] is a combination of the two.

3. Summary and conclusions

To summarize, DLSPP-based microdisk resonator filters, an alternative to microring resonator filters, have been studied by means of vectorial 3D-FEM simulations. We have shown that microdisks feature smaller radiation losses than the respective, footprint-wise, microrings and are therefore advantageous. This advantage is pronounced for small radii, where the radiation losses are significant. Transmission dips due to second-radial-order modes have been observed only for very large disk radii. Their excitation efficiency can be tuned by varying the waveguide width. When only first-radial-order modes are excited (which is mostly the case), the microdisk resonator filter behaves just like a microring resonator filter with the advantage of improved quality factors. Extinction ratios as high as 30 dB have been attained by

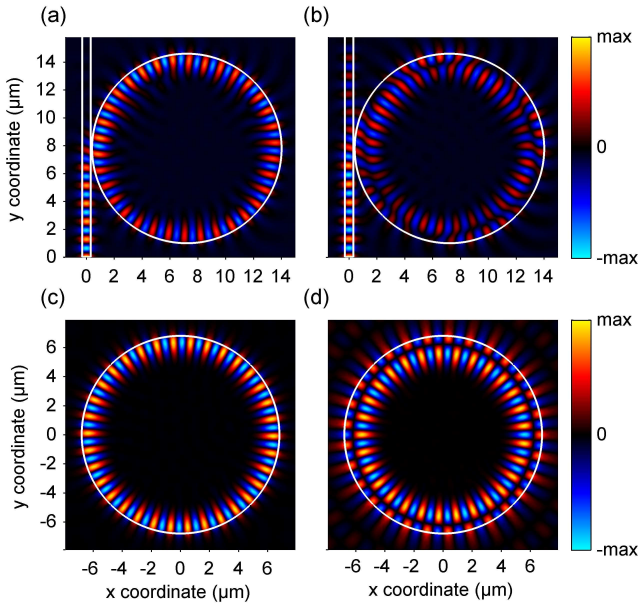

Figure 5: (Color on web only) Real part of E_z for a microdisk filter with $R = 6.8$ μm and $g = 0.1$ μm at a transmission minimum induced by (a) a first-radial-order mode ($\lambda = 1.568$ μm) and (b) a second-radial-order mode ($\lambda = 1.593$ μm). The above minima are clearly marked in Fig. 4. The corresponding modes of the uncoupled resonator are also depicted: (c) $(m, q) = (34, 1)$ and (d) $(m, q) = (29, 2)$. The E_z component is plotted at a xy plane located 10 nm above the metal surface.

properly tuning the gap in each case so as to approach critical coupling.

4. Acknowledgements

This work was supported by the European FP7 project PLATON [Contract No. 249135] and the Greek State Scholarships Foundation (IKY) [Scholarship No. 5613].

References

[1] H. Raether, Surface Plasmons on Smooth and Rough Surfaces and on Gratings, Springer-Verlag, Berlin, 1988.

[2] W. L. Barnes, A. Dereux, T. W. Ebbesen, Surface plasmon subwavelength optics, Nature 424 (2003) 824–830.

[3] S. A. Maier, H. A. Atwater, Plasmonics: Localization and guiding of electromagnetic energy in metal/dielectric structures, J. Appl. Phys. 98 (2005) 011101.

[4] R. Zia, J. A. Schuller, A. Chandran, M. L. Brongersma, Plasmonics: the next chip-scale technology, Mater. Today 9 (2006) 20–27.

[5] E. Ozbay, Plasmonics: Merging photonics and electronics at nanoscale dimensions, Science 311 (2006) 189–193.

[6] T. W. Ebbesen, C. Genet, S. I. Bozhevolnyi, Surface-plasmon circuitry, Phys. Today 61 (2008) 44–50.

[7] T. Nikolajsen, K. Leosson, S. I. Bozhevolnyi, In-line extinction modulator based on long-range surface plasmon polaritons, Opt. Commun. 244 (2005) 455–459.

[8] S. I. Bozhevolnyi, A. Boltasseva, T. Søndergaard, T. Nikolajsen, K. Leosson, Photonic bandgap structures for long-range surface plasmon polaritons, Opt. Commun. 250 (2005) 328–333.

[9] T. Holmgaard, S. I. Bozhevolnyi, Theoretical analysis of dielectric-loaded surface plasmon-polariton waveguides, Phys. Rev. B 75 (2007) 245405.

[10] T. Holmgaard, Z. Chen, S. I. Bozhevolnyi, L. Markey, A. Dereux, A. V. Krasavin, A. V. Zayats, Bend- and splitting loss of dielectric-loaded surface plasmon-polariton waveguides, Opt. Express 16 (2008) 13585–13592.

[11] A. V. Krasavin, A. V. Zayats, Three-dimensional numerical modeling of photonic integration with dielectric-loaded spp waveguides, Phys. Rev. B 78 (2008) 045425.

[12] Z. Chen, T. Holmgaard, S. I. Bozhevolnyi, A. V. Krasavin, A. V. Zayats, L. Markey, A. Dereux, Wavelength-selective directional coupling with dielectric-loaded plasmonic waveguides, Opt. Lett. 34 (2009) 310–312.

[13] T. Holmgaard, Z. Chen, S. I. Bozhevolnyi, L. Markey, A. Dereux, A. V. Krasavin, A. V. Zayats, Wavelength selection by dielectric-loaded plasmonic components, Appl. Phys. Lett. 94 (2009) 051111.

[14] T. Holmgaard, Z. Chen, S. I. Bozhevolnyi, L. Markey, A. Dereux, Dielectric-loaded plasmonic waveguide-ring resonators, Opt. Express 17 (2009) 2968–2975.

[15] O. Tsilipakos, T. V. Yioultsis, E. E. Kriezis, Theoretical analysis of thermally tunable microring resonator filters made of dielectric-loaded plasmonic waveguides, J. Appl. Phys. 106 (2009) 093109.

[16] S. C. Hagness, D. Rafizadeh, S. T. Ho, A. Taflove, FDTD microcavity simulations: Design and experimental realization of waveguide-coupled single-mode ring and whispering-gallery-mode disk resonators, J. Lightwave Technol. 15 (1997) 2154–2165.

[17] D. Rafizadeh, J. P. Zhang, S. C. Hagness, A. Taflove, K. A. Stair, S. T. Ho, R. C. Tiberio, Waveguide-coupled AlGaAs/GaAs microcavity ring and disk resonators with high finesse and 21.6-nm free spectral range, Opt. Lett. 22 (1997) 1244–1246.

[18] K. Djordjev, S.-J. Choi, S.-J. Choi, P. D. Dapkus, Microdisk tunable resonant filters and switches, IEEE Photon. Technol. Lett. 14 (2002) 828–830.

[19] P. Koonath, T. Indukuri, B. Jalali, Verically-coupled micro-resonators realized using three-dimensional sculpting in silicon, Appl. Phys. Lett. 85 (2004) 1018–1020.

[20] P. B. Johnson, R. W. Christy, Optical constants of the noble metals, Phys. Rev. B 6 (1972) 4370–4379.

List of Figure Captions

Figure 1: Schematic of a DLSPP-based microdisk resonator filter. The cross-section at which the output power is calculated is marked as EFGH and is separated by a distance $L = 2R$ from plane ABCD at which the reference power is calculated.

Figure 2: Transmission vs wavelength for a critically coupled microdisk resonator filter with a disk radius of 3.8 μm and a gap of 0.1 μm. The transmission of the respective, footprint-wise, critically coupled microring resonator filter ($R = 3.5$ μm, $g = 0.1$ μm) is also included for comparison purposes.

Figure 3: Transmission vs wavelength for a critically coupled microdisk resonator filter with a disk radius of 5.3 μm and a gap of 0.15 μm. The transmission of the respective, footprint-wise, critically coupled microring resonator filter ($R = 5.3$ μm, $g = 0.2$ μm) is also included for comparison purposes.

Figure 4: Transmission vs wavelength for a microdisk resonator filter with a disk radius of 6.8 μm and a gap of 0.1 μm. Two values for the straight waveguide width, namely 0.6 and 0.5 μm, are considered. Transmission dips due to second-radial-order modes ($q = 2$) are clearly visible.

Figure 5: Real part of E_z for a microdisk filter with $R = 6.8$ μm and $g =$

0.1 μm at a transmission minimum induced by (a) a first-radial-order mode ($\lambda = 1.568$ μm) and (b) a second-radial-order mode ($\lambda = 1.593$ μm). The above minima are clearly marked in Fig. 3. The corresponding modes of the uncoupled resonator are also depicted: (c) $(m, q) = (34, 1)$ and (d) $(m, q) = (29, 2)$. The E_z component is plotted at a xy plane located 10 nm above the metal surface.